Composites Science and Technology 70 (2010) 328–335

Contents lists available at ScienceDirect

Composites Science and Technology

journal homepage: www.elsevier.com/locate/compscitech

Structure–property relationships in isotactic polypropylene/multi-walled carbon nanotubes nanocomposites

E. Logakis [a,*], E. Pollatos [b], Ch. Pandis [a], V. Peoglos [a], I. Zuburtikudis [c], C.G. Delides [d], A. Vatalis [d], M. Gjoka [e], E. Syskakis [f], K. Viras [b], P. Pissis [a]

[a] National Technical University of Athens, Zografou Campus, 15780 Athens, Greece
[b] National and Kapodistrian University of Athens, Chemistry Department, Laboratory of Physical Chemistry, Panepistimiopolis, 15771 Athens, Greece
[c] Technical Education Institute (T.E.I.) of Western Macedonia, Department of Industrial Design Engineering, 50100 Kozani, Greece
[d] Technical Education Institute (T.E.I.) of Western Macedonia, General Department of Sciences, 50100 Kozani, Greece
[e] NCSR "Demokritos", Institute of Materials Science, 15310 Athens, Greece
[f] National and Kapodistrian University of Athens, Physics Department, Section of Solid State Physics, Panepistimiopolis, 15784 Athens, Greece

ARTICLE INFO

Article history:
Received 11 June 2009
Received in revised form 28 October 2009
Accepted 30 October 2009
Available online 6 November 2009

Keywords:
A. Nanocomposites
A. Carbon nanotubes
B. Electrical properties
B. Thermomechanical properties

ABSTRACT

In this work, the influence of multi-walled carbon nanotubes (MWCNT) on electrical, thermal and mechanical properties of CNT reinforced isotactic polypropylene (iPP) nanocomposites is studied. The composites were obtained by diluting a masterbatch of 20 wt.% MWCNT with a low viscous iPP, using melt mixing. The morphology of the prepared samples was examined through SEM, Raman and XRD measurements. The effect of MWCNT addition on the thermal transitions of the iPP was investigated by differential scanning calorimetry (DSC) measurements. Significant changes are reported in the crystallization behavior of the matrix on addition of carbon nanotubes: increase of the degree of crystallinity, as well as appearance of a new crystallization peak (owing to trans-crystallinity). Dynamic mechanical analysis (DMA) studies revealed an enhancement of the storage modulus, in the glassy state, up to 86%. Furthermore, broadband dielectric relaxation spectroscopy (DRS) was employed to study the electrical and dielectric properties of the nanocomposites. The electrical percolation threshold was calculated 0.6–0.7 vol.% MWCNT from both dc conductivity and dielectric constant values. This value is lower than previous mentioned ones in literature in similar systems. In conclusion, this works provides a simple and quick way for the preparation of PP/MWCNT nanocomposites with low electrical percolation threshold and significantly enhanced mechanical properties.

1. Introduction

The reinforcement of polymers with nano-scaled fillers developed a new class of advanced multifunctional materials with improved properties, used in many fields ranging from microelectronics to aerospace [1,2]. Among nanofillers, carbon nanotubes (CNT) are an especially attractive class of inclusions because of their exceptional mechanical, thermal, and electrical properties. On the other hand, among the most versatile polymer matrices are polyolefins, such as polypropylene, because of their good balance between properties and cost, low density and ease in processibility [3]. For further enhancing of properties, like mechanical improvement, the addition of carbon nanotubes is widely investigated in literature [4]. Apart from mechanical reinforcement, one key interest is the development of conductive polymer composites, preferably at low concentration of CNT, by taking advantage of their high aspect ratio (~1000), and retaining in that way the good processability of the host matrix [5]. Such types of nanocomposites are suitable for numerous applications, which include antistatic devices, capacitors, materials for electromagnetic interference (EMI) shielding, and sensors [6].

Several processing methods are available for the production of polymer/CNT composites, such as melt mixing, solution casting and in situ polymerization [7]. Among them, melt mixing is particular desirable as it combines speed with simplicity. Furthermore, it is free of solvents and contaminants and the required equipment is already available in the plastic industry. In all the techniques mentioned above, a homogeneous dispersion and good interfacial adhesion are crucial for the successful preparation of nanocomposites [7,8]. Additionally, usage of preformed masterbatches, usually containing 10–20 wt.% nanotubes, facilitates even more the processing as it prohibits any contact with the nanotubes in dust form, which could be potentially hurtful [9]. A recent, comprehensive study which summarizes the benefits and recent work in systems obtained by dilution of commercially available masterbatches is given in Ref. [10].

* Corresponding author. Tel.: +30 210 7722974.
E-mail address: logmanos@central.ntua.gr (E. Logakis).

0266-3538/$ - see front matter © 2009 Elsevier Ltd. All rights reserved.
doi:10.1016/j.compscitech.2009.10.023

This work follows a previous one by Mičušik et al. [11], where various types of polypropylenes differing in melt flow indexes (MFI = 2.0, 8.0, and 11.8 g/10 min) were used to dilute the same masterbatch like here (PP having MFI = 11.8 g/10 min and containing 20 wt.% MWCNT, obtained from Hyperion Catalysis International) by melt mixing technique (mixing conditions: 190 °C, 35 rpm, 10 min). It was shown in that article, that the lowest percolation threshold values ($p_c \approx 1.1$ vol.%) were achieved when the dilution of the masterbatch was done using the PP grades with lower viscosity (MFI = 8.0 and 11.8 g/10 min), compared to high viscous PP (MFI = 2.0 g/10 min, $p_c \approx 2.0$ vol.%) [11]. SEM, TEM and rheology measurements were consistent with that result, showing a better state of dispersion in the low viscous systems. Having in mind these results, in this work the dilution was performed by using an even less viscous PP (MFI = 35.0 g/10 min). Additionally, the mixing conditions were altered. In particular, the mixing speed was much higher (200 rpm), the mixing time was significantly prolonged (over 30 min), whereas the mixing temperature was kept almost the same (180 °C) in order to prevent any decomposition of the polymer. We show in the present paper that these alterations, in the polymer matrix selection for the dilution and in the mixing conditions, lead to further decrease of p_c ($p_c \approx 0.6$ vol.%).

Generally, the higher the mixing speed, time and temperature are, the better dispersion of CNT is achieved. The drawback of the increase of all the mentioned above parameters is the decrease of the aspect ratio of the fillers [8], a factor which is crucial for the electrical percolation threshold [12]. In this work, the low viscosity in the melt, due to the high MFI of the polymer used, allowed us to conduct a tenacious mixing of CNT with the polymer without destroying CNT, as the low p_c value indicates.

Additionally, significant enhancement of the storage modulus (up to 86% in the glassy state) was observed for the samples with high amounts of CNT (3 and 5 wt.% CNT), as shown by dynamic mechanical analysis (DMA) measurements. The enhancement of the mechanical properties is correlated with the appearance of trans-crystallinity structure in PP by the addition of carbon nanotubes, indicated by differential scanning calorimetry (DSC). This crystalline layer around CNT seems to intervene between the matrix and the embedded nanotubes, transferring in that way the load from the amorphous phase to the stiff CNT.

2. Experimental

2.1. Materials

Masterbatch granules of polypropylene containing 20 wt.% of MWCNT, obtained from Hyperion Catalysis International (USA), were used as components for the preparation of the thermoplastic composites with lower CNT contents. The nanoubes are produced by chemical vapour deposition method (CVD). The outside diameter (D) of the tube is approximately 10 nm and the length (L) is over 10 μm giving a high aspect ratio (L/D) of about 1000. The density is approximately 1.74 g/cm^3, as it is calculated by Raman spectroscopy (Section 3.3). The nanocomposites were prepared by melt mixing the starting masterbatch with a low viscous isotactic polypropylene (iPP) (melt flow index: 35 g/10 min (230 °C/2.16 kg, ASTM D 1238), M_n: 50,000, M_w: 190,000) obtained from Aldrich Polymer Products. The mixing was done in a co-rotating, conical, twin-screw micro-extruder/compounder (ThermoHaake MiniLab™) at 180 °C, for over 30 min and at a mixing speed of 200 rpm in N_2 atmosphere. Slabs with a thickness of 0.5 mm were prepared by compression moulding of the mixed composites using a custom hydraulic press at 15 MPa for 5 min initially and at 30 MPa for additional 5 min, while the temperature was kept at 170 °C. Then, the temperature would be decreased from 170 °C to 40 °C at a sufficiently low rate. The final obtained concentration of MWCNT in the prepared nanocomposites varies from 0.3 to 5.0 wt.%.

2.2. Characterization

The morphology of iPP/MWCNT composites was observed using a scanning electron microscopy (SEM) (FE Inspect SEM, Philips, Netherlands) operating with an acceleration voltage of 20 kV. SEM samples were cryo-fractured in liquid nitrogen and their fractured surface was sputtered with gold before taking the images to prevent charging.

X-ray diffraction (XRD) patterns were taken on a Siemens D500 diffractometer, using Cu Kα radiation of a wavelength of $\lambda = 0.154$ nm. Measurements were performed over the range 2θ from 5° to 55°, at steps of 0.04° and counting time of 5 s.

Raman spectra were recorded on a Perkin–Elmer GX Fourier Transform spectrometer. A diode pumped Nd:YAG laser exciting at 1064 nm was used. The scattered radiation was collected at an angle of 180° to the incident beam. Spectra were recorded at a laser power of 30 mW at the sample with a resolution of 4 cm^{-1} and an interval of 2 cm^{-1}. In order to obtain a good signal to noise ratio, 1000 scans were co-added for the spectra. The Raman spectra were taken in the spectral region 100–3500 cm^{-1}.

Differential scanning calorimetry (DSC) measurements were carried out in the temperature range −70 to 180 °C, using a Perkin–Elmer Pyris 6 apparatus. A cooling rate of 10 K/min and a heating rate of 10 K/min were used. The weight of the samples varied from 4 to 6 mg. It is noted that iPP and its composite samples containing various MWCNT amounts were formerly heated at 180 °C for 5 min in order to remove the previous thermal history. All measurements were carried out in nitrogen atmosphere.

The mechanical properties of the prepared materials were examined by dynamic mechanical thermal analysis (DMTA) at a frequency of 10 Hz from room temperature up to 200 °C, using a Polymer Laboratories dynamic mechanical thermal analyzer MK III. A scanning rate of 2 °C/min and a strain of 4× were used.

The electrical and dielectric properties of the prepared materials were studied by employing dielectric relaxation spectroscopy (DRS). In this technique the sample is placed between the plates of a capacitor, an alternate voltage is applied, and the response of the system is studied. By measuring the complex impedance ($Z^* = Z' - iZ''$) of the circuit the complex permittivity ($\varepsilon^* = \varepsilon' - i\varepsilon''$) arises from the following equation [13]:

$$\varepsilon^*(\omega) = \frac{1}{i\omega Z^*(\omega) C_0} \tag{1}$$

where ω is the angular frequency ($\omega = 2\pi f$) of the applied electric field and C_0 the equivalent capacitance of the empty capacitor. The frequency-dependent ac conductivity (real part, σ') is then obtained from the following equation [13]:

$$\sigma'(\omega) = \varepsilon_0\, \omega\, \varepsilon''(\omega) \tag{2}$$

where $\varepsilon_0 = 8.85 \times 10^{-12}$ F m^{-1} is the permittivity of free space. In this work, DRS measurements were carried out in a wide frequency range of 10^{-2}–10^6 Hz by means of a Novocontrol Alpha analyzer (Germany).

3. Results and discussion

3.1. Morphological characterization

In Fig. 1 SEM images for the nanocomposites containing 1.0 and 3.0 wt.% MWCNT are presented.

The micrographs show that MWCNT are uniformly dispersed in the polymer matrix with small amount of agglomerates, indicating

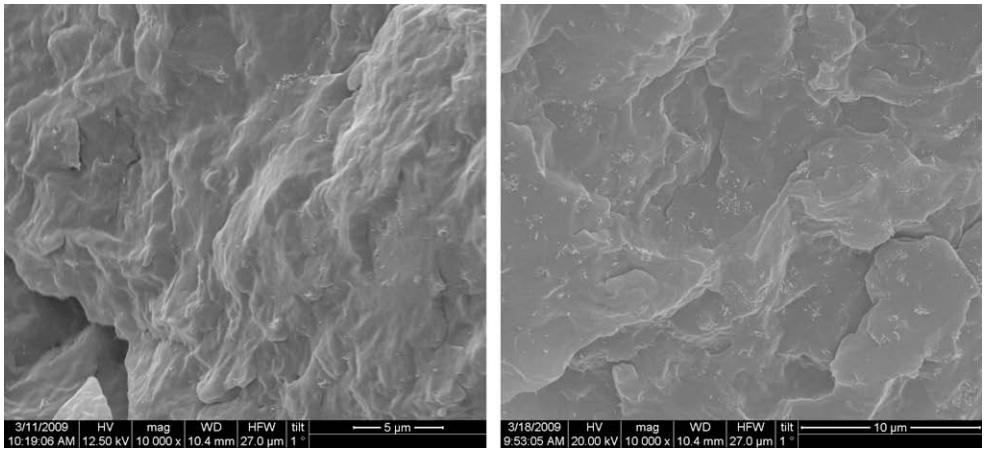

Fig. 1. SEM micrographs for the nanocomposites containing 1 wt.% (left) and 3 wt.% (right) MWCNT.

that the masterbatch dilution technique using melt mixing was appropriate in order to obtain a homogeneous distribution of nanotubes in the polymer matrix. Thus, these composites are suitable for the investigation of the influence of nanotube addition on the crystallization behavior and the mechanical properties of the polypropylene matrix, and to study electrical percolation aspects.

3.2. X-ray diffraction

The addition of nanoparticles in the iPP matrix can cause changes in the crystallization rate of the polymer and even induce changes in its crystal conformation [14]. To examine this possibility X-ray diffraction measurements carried out. Fig. 2 shows the XRD patterns of pure iPP and iPP/MWCNTs composites. Both pure iPP and iPP/MWCNT nanocomposites display characteristic diffracting peaks at $2\theta = 13.9°$, 16.7°, 18.3° and 21.6° corresponding to the planes (1 1 0), (0 4 0), (1 3 0) and (1 1 1) of its α-phase crystallite and exhibit complete absence of the β-crystal form, which shows two strong peaks at 2θ of 16.2° and 21.2° [14–16]. While certain nucleating agents can promote β-crystal formation in PP [16,17], this study shows only the α-crystal formation in iPP/MWCNT composites. This result is consistent with a previous study in PP/SWCNT and PP/MWCNT systems [15,18].

3.3. Raman spectroscopy

Raman spectra of polymer/CNT composites have attracted a lot attention, both theoretically [19,20] and experimentally [21,22], and has become a tool for the study and characterization of CNT nanocomposites, in order to identify carbon nanotubes (i.e. graphitization, inner diameter and density), access their dispersion in polymers, evaluate nanotube/matrix interactions and detect polymer phase transitions. Raman spectra of polymer/CNT composites typically show intense peaks in the spectral ranges of 1200–1700 cm^{-1} and 140–200 cm^{-1}. Fig. 3 shows the high frequency Raman spectra of MWCNT and the nanocomposites for several nanotube concentrations (0.5, 1, 3 and 5 wt.%). Two characteristics peaks are presented: the first centered at 1306 cm^{-1} assigned to the D band and derived from disordered graphite structures, and the second centered at 1594 cm^{-1} assigned to the G band and is attributed to modes with neighboring C atoms vibrating out-of-phase parallel to the surface of the cylinder (tangential modes) which are related to the E_{2g} phonon at about 1580 cm^{-1} in graphite [23].

By increasing the nanotube concentration in the polymer matrix, the G band is upshifted, as shown in Fig. 3. The shifting of the band to higher frequencies can be attributed to the disentanglement of nanotubes and subsequent dispersion in the iPP matrix, as a consequence of polymer penetration into the nanotubes bundles during melt mixing process. The latter is expected to contribute significantly to the influence of the crystallization, due to the increase of the formation of nucleant agents which favor the crystallization process, as it will be discussed in Section 3.4. Similar upshifting of the G band has been reported for SWCNT/polypropylene [24] and reinforced epoxy resins [25], as well as for polyethylene matrix [26].

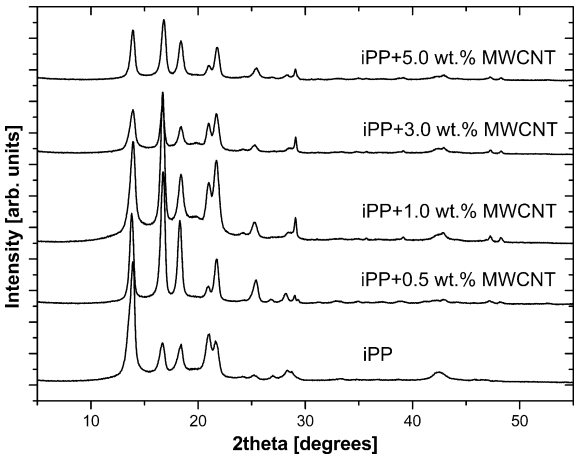

Fig. 2. XRD patterns for the pure iPP and for the nanocomposites indicated on the plot.

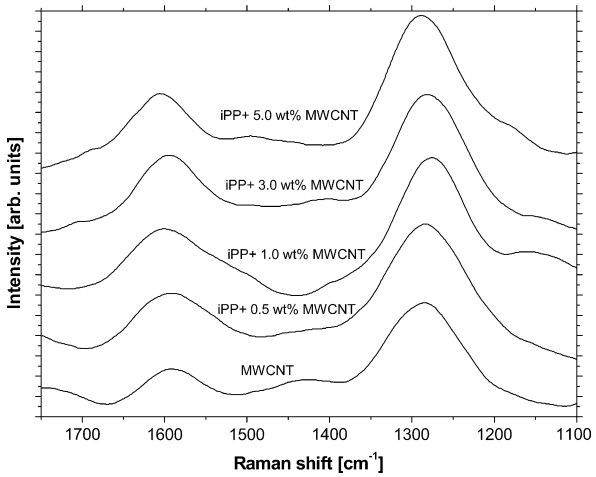

Fig. 3. High frequency Raman spectra of MWCNT and iPP/MWCNT nanocomposites.

Using the peak height Raman intensities of the G and D bands in the equation $I_G/(I_G + I_D) \times 100\%$ the degree of graphitization of carbon nanotubes was found 43% [27].

The low-energy bands in Raman spectra are attributed to a radial breathing mode (RBM) where all C atoms are subject to an in-phase radial displacement, associated with a symmetric movement of all carbon atoms in the radial direction. The frequency of RBM mode is proportionally to the inverse of the tube inner diameter $(1/d)$ according to the equation: $\omega_{RBM} = 223.5/d + 12.5$, where ω_{RBM} is given in cm^{-1} and d in nm [23].

A prominent RBM band at about 163 cm^{-1} was recorded in spectra of MWCNT and in iPP/MWCNT composites. Band component analysis (Fig. 4) gave three main bands at 161, 163 and 167 cm^{-1} which correspond to nanotubes with inner diameters 1.50, 1.48 and 1.44 nm respectively. Using the mean inner diameter value in the equation $\rho_{CNT} = \rho_g(D^2 - d^2)/D^2$ [27], where ρ_g and D are the density of graphite and the outer diameter respectively, the density of carbon nanotubes ρ_{CNT} was found 1.74 g/cm^3.

3.4. Effects of MWCNT addition on the thermal transitions of iPP

The effects of MWCNT addition on the thermal properties of the host matrix (iPP), crystallization in Figs. 5 and 6 and melting in Fig. 7, were examined by employing DSC. Fig. 5 shows the thermograms for iPP and selected iPP/MWCNT nanocomposites at a cooling rate of 10 K/min, where the crystallization exotherms are observed. For the iPP matrix only a single crystallization peak ($T_{c,1}$) appears at 108.6 °C. For the iPP/MWCNT nanocomposites the $T_{c,1}$ peak shifts gradually to higher temperatures, as the amount of MWCNT increases, indicating that carbon nanotubes act as nucleating agents. This behavior has been reported previously in literature for polypropylene [24,28–30] and other semicrystalline matrixes, such as polyamide [31–34] and polystyrene [35]. The observed increase of $T_{c,1}$ is more pronounced at low nanotubes contents ($T_{c,1}$ is increased by 13 °C on addition of only 0.5 wt.% MWCNT) and becomes weaker as the amount of CNT increases (Table 1). Additionally, the crystallization peak appears to be narrower in the case of nanocomposites. The degree of crystallinity (X_c) of iPP is calculated from the melting thermograms by the following equation:

$$X_c\ (\%) = \frac{\Delta H_m}{(1-\varphi)\Delta H_0} \times 100 = \frac{\Delta H_m^*}{\Delta H_0} \times 100 \qquad (3)$$

where ΔH_m is the heat of fusion of the measured sample, ΔH_0 is the heat of fusion for 100% crystalline iPP and φ is the weight fraction of CNT in the nanocomposites. ΔH_0 was taken equal to 209 J/g [36]. The results listed in Table 1 show a slight increase of X_c as the amount of CNT increases. The relatively high cooling rate of 10 K/min gives limited time to the polymer to be crystallized, and, as a result, the addition of external nucleating sites, such as carbon

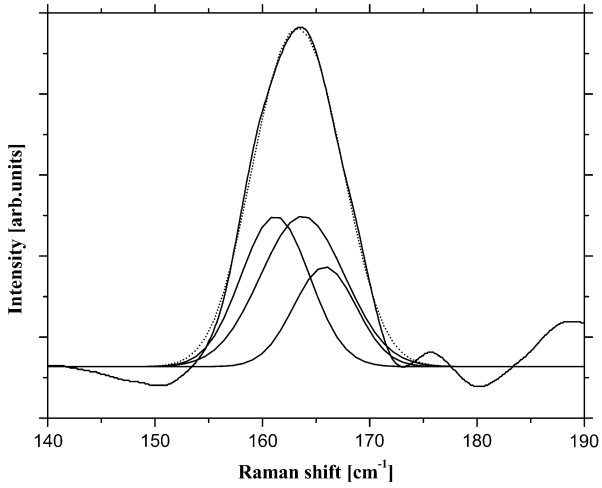

Fig. 4. Low frequency Raman spectrum of iPP/3.0 wt.% MWCNT composite.

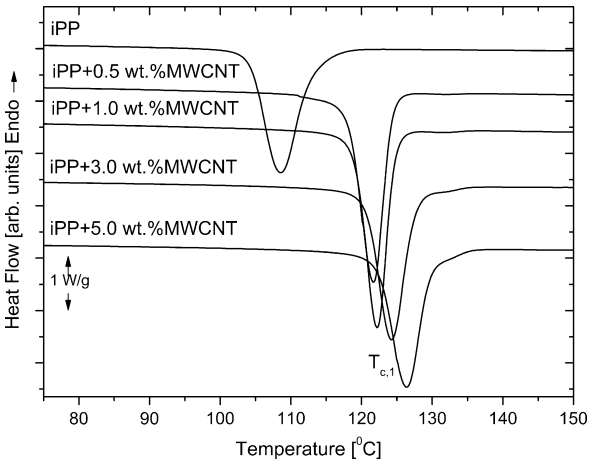

Fig. 5. Crystallization thermograms for pure iPP and the nanocomposites indicated on the plot (cooling rate: 10 K/min).

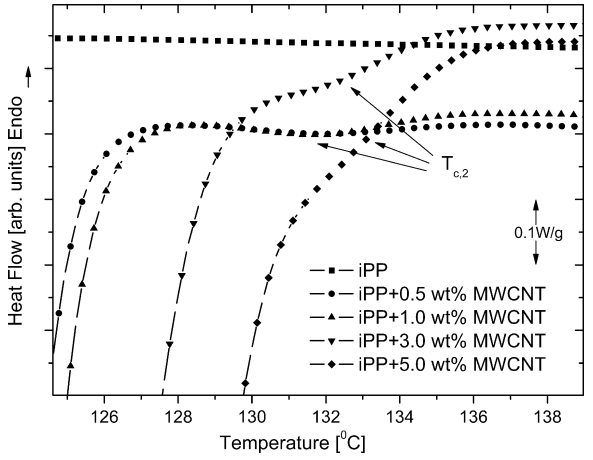

Fig. 6. Appearance of $T_{c,2}$ peak on addition of MWCNT.

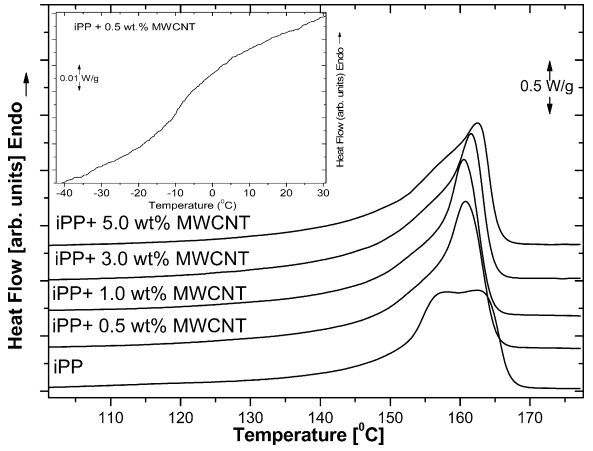

Fig. 7. Melting thermograms for pure iPP and the nanocomposites indicated on the plot (heating rate: 10 K/min). The inset shows, as an example, the glass transition region for iPP/0.5 wt.% MWCNT.

Table 1
Melting temperature (T_m), heat of fusion (ΔH_m), heat of fusion normalized to the polymer mass (ΔH_m^*), degree of crystallinity (X_c) and crystallization temperature ($T_{c,1}$) for the pure iPP matrix and iPP/MWCNT nanocomposites. It is noted that the errors in temperatures are estimated to ±0.5 °C, whereas in enthalpies and in degree of crystallinity are in the order of 5%.

Sample	Melting				Crystallization
	T_m (°C)	ΔH_m (J/g)	ΔH_m^* (J/g)	X_c (%)	$T_{c,1}$ (°C)
iPP	158.2 and 162.4	88	88	42	108.6
iPP/0.5 wt.% MWCNT	160.8	92	93	44	121.7
iPP/1.0 wt.% MWCNT	160.5	93	94	45	122.3
iPP/3.0 wt.% MWCNT	161.6	92	95	45	124.4
iPP/5.0 wt.% MWCNT	162.4	89	93	45	126.4

nanotubes, leads to an increase of crystallization rate and consequently to an increase of X_c.

Another alteration in the crystallization of iPP is the appearance of a new crystallization peak ($T_{c,2}$) by the addition of carbon nanotubes, at higher temperatures and especially for the highly loaded samples (3 and 5 wt.% MWCNT) (Fig. 6). The origin of this peak is attributed to trans-crystallinity. In this special kind of morphology, crystallization begins on the surface of a flat or fibril nucleating object and results in a one-dimensional (columnar) growth of crystallites in a direction parallel to the normal of the surface [37]. This structure begins to develop on the walls of CNT before the most common supermolecular structure of spheroulites ($T_{c,1}$ peak), which is observed thereupon during the cooling. The trans-crystallinity structure has been reported in various conventional polymer/fiber composites [38,39] and recently in nanocomposites. In particular, in Refs. [34,40] similar results were obtained by DSC in polyamide 6/MWCNT composites. Additionally, in Refs. [41,42] polarized light microscopy and transmission electron microscopy results in iPP/MWCNT show this structure even more convincingly. The existence of this layer is of a grate importance, as it seems to affect the mechanical properties of the nanocomposites (see Section 3.5).

In Fig. 7 melting thermograms (second heat) are presented for the iPP and its nanocomposites at a heating rate of 10 K/min. For the pure iPP two main melting peaks are located at 158.2 and 162.4 °C. The peak at high temperatures is attributed to the melting of α-crystals, whereas the broad peak at the temperature range 150–160 °C can be due to the melting of β-crystals, or smaller or imperfect α-crystals [15]. The latter is the case here, since X-ray diffraction patterns do not show any presence of β-crystals (see Section 3.2). In the nanocomposites the melting peaks are narrower, a result which suggest a narrower crystallite size distribution as compared to the pure matrix. The higher thermal conductivity of CNT, as compared to that of the polymer, allows heat to be more evenly distributed in the nanocomposites, and explains, at least in part, the sharper crystallization and melting peaks [15]. As concerns the glass transition of the amorphous iPP phase (an example is given in the inset to Fig. 7 for the sample iPP + 0.5 wt.% MWCNT), no significant changes are observed either to the position of the glass transition temperature ($T_g \approx -7$ °C) or to the heat capacity jump (ΔC_p).

3.5. Mechanical properties

The mechanical properties of the nanocomposites were analyzed with dynamic mechanical thermal analysis (DMTA). The steps and the peaks which appear in the dynamic storage modulus (E') (Fig. 8) and in tangent delta (tan δ) (Fig. 9), respectively, correspond to the glass transition of iPP. E' increases in the glassy state on addition of carbon nanotubes (Table 2). This increase is rather small for the samples containing low amounts of CNT and becomes significant for the highly loaded samples (3 and 5 wt.% MWCNT). In particular, E' increases from 3.6 GPa for pure iPP, to 6.4 GPa for the

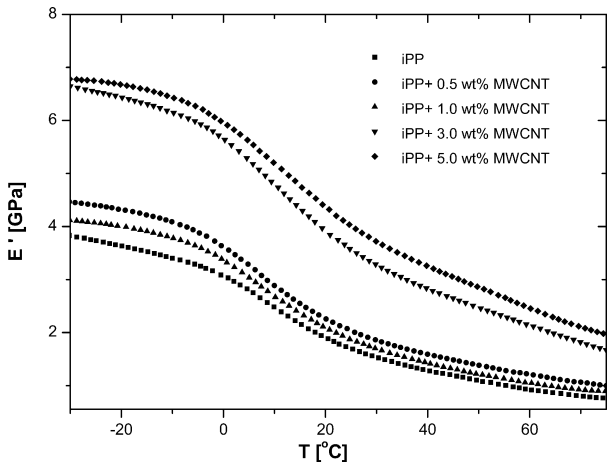

Fig. 8. Storage modulus versus temperature for the pure iPP and for the nanocomposites indicated on the plot.

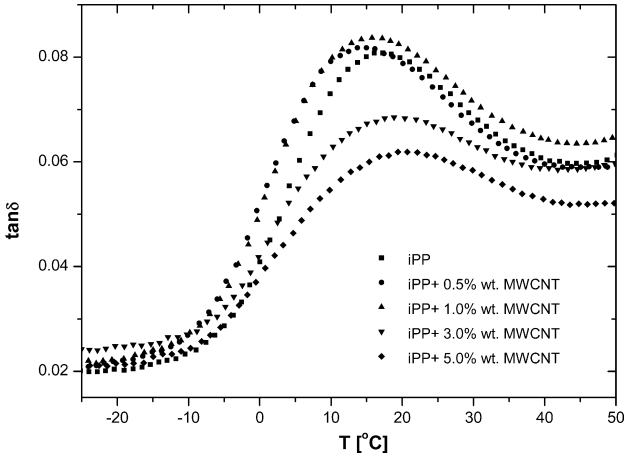

Fig. 9. Tan δ versus temperature for the pure iPP and for the nanocomposites indicated on the plot.

Table 2
Dynamic storage modulus (E') in the glassy and in the rubbery state for the pure iPP matrix and iPP/MWCNT nanocomposites. It is noted that the error in E' values is in the order of 1% (estimated after the repetition of each measurement for three times).

Sample	E' in the glassy state (at −20 °C) (GPa)	E' in the rubbery state (at 60 °C) (GPa)
iPP	3.6	0.9
iPP/0.5 wt.% MWCNT	4.3	1.2
iPP/1.0 wt.% MWCNT	4.0	1.0
iPP/3.0 wt.% MWCNT	6.4	2.1
iPP/5.0 wt.% MWCNT	6.7	2.5

nanocomposite with 3.0 wt.% MWCNT, and to 6.7 GPa for the nanocomposite with 5.0 wt.% MWCNT, representing 78% and 86% improvement, respectively (Table 2).

This enhancement of the mechanical properties is correlated with the appearance of trans-crystallinity structure in iPP on addition of carbon nanotubes, as indicated by the DSC results. As it was shown in Section 3.4, this structure is present in all the nanocomposites, but it becomes significant for the same samples which exhibit significant enhancement in their mechanical properties. This crystalline layer around CNT seems to intervene between the matrix and the embedded nanotubes, transferring in that way effectively the load from the amorphous phase to the stiff CNT [43]. Similar findings have been obtained in our previous work in PA6/MWCNT systems [34], but it was not possible there to identify the reason for the observed enhancement, as the appearance of the trans-crystallization structure was combined with the conversion of the γ phase crystals of PA6 to α, which exhibit improved mechanical properties. Here, any effects stemming from crystallite conversion can be excluded, as it was shown by XRD. Additionally, the observed increase in the degree of crystallinity of iPP is negligible (Table 1), compared to the large increase of E', and cannot account for the latter. Finally, it is mentioned that the enhancement of E' is retained in the rubbery state also, as it is shown in Table 2.

3.6. Electrical properties

Fig. 10 shows the frequency (f) dependence of the real part of the complex electrical conductivity $\sigma'(f)$ for various MWCNT weight contents measured at room temperature. Two distinct behaviors, depending on the nanotubes concentration, are observed. Ac conductivity increases linearly as frequency increases for the samples with compositions between 0.3 and 1 wt.% MWCNT as well as for neat iPP, which is typical for insulating materials. Contrary, the samples with loadings of at least 1.5 wt.% MWCNT exhibit a dc plateau where σ' is independent of frequency below a critical frequency (f_c). For the samples with high MWCNT contents the independence of ac conductivity on frequency, which is characteristic for conductive materials, is extended in the whole frequency range. It is clearly seen that the transition from insulating to conducting phase takes place between 1.0 and 1.5 wt.% of MWCNT. Thus, the percolation threshold (p_c), being the critical composition of conducting inclusions where the first network is formed, is located between these two values.

For the exact calculation of p_c the well known scaling low from percolation theory [44] was used to the experimental data in Fig. 11:

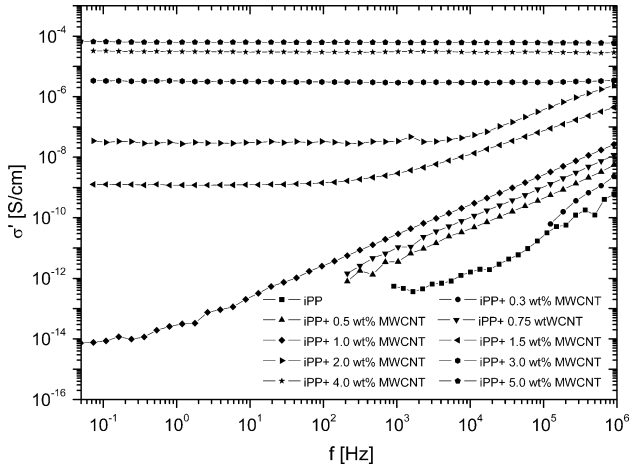

Fig. 10. Conductivity (σ') versus frequency (f) at room temperature for the samples indicated on the plot.

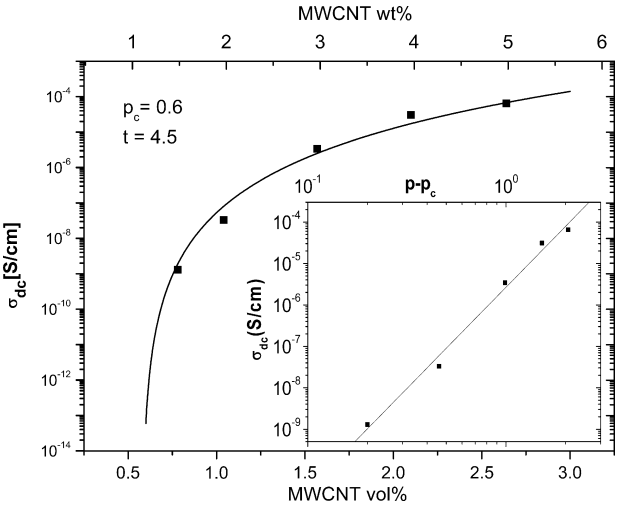

Fig. 11. σ_{dc} versus MWCNT vol.% (and wt.%) concentration for nanocomposites above p_c. The inset shows a log–log plot of σ_{dc} versus $(p - p_c)$ with $t = 4.5$ and $p_c \approx 0.6$ vol.%.

$$\sigma_{dc} \sim (p - p_c)^t \tag{4}$$

where σ_{dc} is the dc conductivity (as obtained from the plateau values of the conductive samples in Fig. 10), p is the volume fraction of the filler, and t is the critical exponent, which is related with the dimensionality of the investigated system. The conversion of wt.% to vol.% concentrations was done using the following equation:

$$\varphi_{\text{vol}} = \frac{1}{1 + \frac{\rho_{\text{CNT}}}{\rho_{\text{Pol}}}\left(\frac{1}{\varphi_{\text{wt}}} - 1\right)} \tag{5}$$

where φ_{vol} and φ_{wt} are the volume and weight fraction of MWCNT, respectively. The mass densities of MWCNT and iPP are $\rho_{\text{CNT}} = 1.74\ \text{g/cm}^3$ (as obtained by Raman spectroscopy) and $\rho_{\text{Pol}} = 0.9\ \text{g/cm}^3$. A value of $t \approx 2.0$ is predicted theoretically for a statistical percolation network in three dimensions [45]. The best linear fit for σ_{dc} versus p was achieved for $p_c = 0.6 \pm 0.1$ vol.% (or 1.2 wt.%) and $t = 4.5 \pm 0.2$ (Fig. 11). In the inset to Fig. 11 σ_{dc} versus $(p - p_c)$ is plotted and shows the estimation of percolation threshold in a different representation. The calculated value for the exponent t is high and deviates from the theoretically expected. In any case, such high values for t have been mentioned before in literature in many systems. Many examples and reasons for this discrepancy are given in Refs. [5,46] and in references there into.

Dielectric relaxation spectroscopy gives us the opportunity to study and estimate the percolation threshold from the dielectric constant (ε') values of the insulating samples which are below the percolation threshold. Thus, an alternative route for the estimation of p_c is provided, controlling in that way the correctness of the results obtained by the conventional method (σ_{dc} versus p). A third way, through the critical frequency (f_c), has been also presented in Ref. [46]. This third method is not applicable here, as the transition from the insulating to the conducting phase is rather sharp and consequently f_c can be read only in two samples.

Fig. 12 presents the real part of the complex permittivity (ε') versus frequency (f) for the samples which exhibit insulating behavior. The first concentration above p_c (1.5 wt.% MWCNT) is also included in order to show the difference which is observed at p_c. As it is seen, ε' increases as the amount of MWCNT in the composites increases. Polypropylene, as a non-polar polymer, does not exhibit dielectric relaxation mechanisms; therefore the real part of dielectric function is practically frequency invariant in the whole frequency range. It is noted that in the case of polymers with

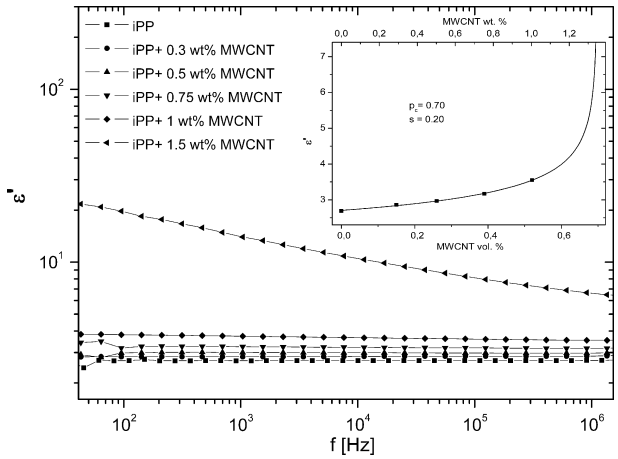

Fig. 12. Real part of the dielectric function (ε') as a function of frequency (f) for the samples indicated on the plot. The inset shows the estimation of p_c according to Eq. (5).

polar groups relaxation mechanisms appear in the spectra in the form of steps [13]. This increase in dielectric constant, still remaining below p_c, is beneficial for the development of materials (known as high-k materials) with potential applications in microelectronics. The sharp increase in ε' values for the sample containing 1.5 wt.% indicates the percolation threshold. Consequently, p_c lies in between 1.0 and 1.5 wt.% MWCNT. For the exact calculation of p_c, ε' is plotted against vol.% MWCNT concentration (see inset to Fig. 12). Generally, ε' values are taken at a high frequency (here at 1 MHz) in order to exclude any dipolar contribution to the dielectric constant. Here $f = 1$ MHz was chosen, although, due to the lack of polar groups in polypropylene chains, ε' is practically constant in the whole frequency range. Fitting of the scaling low from percolation theory [47]:

$$\varepsilon' \sim (p_c - p)^{-s} \tag{6}$$

to the experimental data (see inset to Fig. 12) gave the following values: $p_c = 0.7 \pm 0.1$ vol.% and $s = 0.20 \pm 0.03$. Like in Eq. (3), s is a critical exponent which is related with the dimensionality of the percolative network. The obtained value of s diverges from the commonly accepted value of 0.7 for three-dimensional percolation. Similar low values of s have been previously reported [48,49] for percolative systems containing prolate inclusions.

In summary, both fits of σ_{dc} versus p (Fig. 11) and of ε' versus p (inset to Fig. 12) data gave p_c values in consistency to each other. The estimated percolation threshold is lower than previous mentioned ones in literature, as concerns semicrystalline polymer/CNT composites obtained by dilution of a commercially available masterbatch (1.1 vol.% in PP/MWCNT [11], 2.1 vol.% or 4.5 wt.% in PP/MWCNT [50], 1.7 vol.% or 2.6 wt.% in polyamide 6/MWCNT [46]). Comparable values or even lower have also been reported, however in systems where the matrix was an amorphous polymer (0.5–1.0 wt.% in polycarbonate/MWCNT [51]).

4. Conclusions

This work provides a simple and quick way for the preparation of PP/MWCNT nanocomposites, by diluting a commercial masterbatch through melt mixing technique. The nanocomposites exhibit a low percolation threshold of about 0.6 vol.%, as it was calculated by both dc conductivity and dielectric constant values. This threshold is significant lower than previously reported results in similar systems, and it was achieved by making the appropriate selection of the dilution polymer, as well as the mixing conditions in the melt. The latter is combined with significantly enhanced mechanical properties, especially in the highly loaded samples. The enhancement is correlated with the appearance of a crystalline layer around CNT walls due to trans-crystallinity, as it was shown by DSC. This interphasial layer seems to intervene between the matrix and the embedded nanotubes, transferring in that way effectively the load from the amorphous phase to the stiff CNT.

Acknowledgements

This work has been funded by the project PENED 2003. The project is cofinanced 75% of public expenditure through EC – European Social Fund, 25% of public expenditure through Ministry of Development – General Secretariat of Research and Technology and through private sector, under measure 8.3 of OPERATIONAL PROGRAMME "COMPETITIVENESS" in the 3rd Community Support Programme.

References

[1] Thostenson ET, Li C, Chou TW. Nanocomposites in context. Compos Sci Technol 2005;65:491–516.
[2] Hussain F, Hojati M, Okamoto M, Gorga RE. Polymer–matrix nanocomposites, processing, manufacturing, and application: an overview. J Compos Mater 2006;40:1511–65.
[3] Mihaela M, Olaru A. In: Cornelia V, editor. Handbook of polyolefins. Marcel Dekker Inc.; 1993. p. 267–90.
[4] Zhang WD, Shen L, Phang IY, Liu T. Carbon nanotubes reinforced nylon-6 composite prepared by simple melt-compounding. Macromolecules 2004;37:256–9.
[5] Bauhofer W, Kovacs JZ. A review and analysis of electrical percolation in carbon nanotube polymer composites. Compos Sci Technol 2009;69:1486–98.
[6] Breuer O, Sundararaj U. Big returns from small fibers: a review of polymer/carbon nanotube composites. Polym Compos 2004;25:630–45.
[7] Grossiord N, Loos J, Regev O, Koning CE. Toolbox for dispersing carbon nanotubes into polymers to get conductive nanocomposites. Chem Mater 2006;18:1089–99.
[8] Andrews R, Jacques D, Minot M, Rantell T. Fabrication of carbon multiwall nanotube/polymer composites by shear mixing. Macromol Mater Eng 2002;287:395–403.
[9] Muller J, Huaux F, Lison D. Respiratory toxicity of carbon nanotubes: how worried should we be? Carbon 2006;44:1048–56.
[10] Prashantha K, Soulestin J, Lacrampe MF, Krawczak P, Dupin G, Claes M. Masterbatch-based multi-walled carbon nanotube filled polypropylene nanocomposites: assessment of rheological and mechanical properties. Compos Sci Technol 2009;69:1756–63.
[11] Mičušik M, Omastová M, Krupa I, Prokeš J, Pissis P, Logakis E, et al. A comparative study on the electrical and mechanical behaviour of multi-walled carbon nanotube composites prepared by diluting a masterbatch with various types of polypropylenes. J Appl Polym Sci 2009;113:2536–51.
[12] Garboczi EJ, Snyder KA, Douglas JF. Geometrical percolation threshold of overlapping ellipsoids. Phys Rev E 1995;52:819–28.
[13] Kremer F, Schoenhals A. Broadband dielectric spectroscopy. Germany: Springer; 2002. p. 245.
[14] Bikiaris D, Vassiliou A, Chrissafis K, Paraskevopoulos KM, Jannnakoudakis A, Docoslis A. Effect of acid treated multi-walled carbon nanotubes on the mechanical, permeability, thermal properties and thermo-oxidative stability of isotactic polypropylene. Polym Degrad Stabil 2008;93:952–67.
[15] Bhattacharyya AR, Sreekumar TV, Liou T, Kumar S, Ericson LM, Hauge RH, et al. Crystallization and orientation studies in polypropylene/single wall carbon nanotube composite. Polymer 2003;44:2373–7.
[16] Ellis G, Gomez MA, Macro C. Mapping the crystalline morphology of isotactic polypropylene by infrared microscopy. Internet J Vib Spectrosc 2001;5 (4th ed., section 5).
[17] Seo MK, Lee JR, Park SJ. Crystallization kinetics and interfacial behaviours of polypropylene composites reinforced with multi-walled carbon nanotubes. Mater Sci Eng A 2005;404:79–84.
[18] Satapathy BK, Ganß M, Weidisch R, Pötschke P, Jehnichen D, Keller T, et al. Ductile-to-semiductile transition in PP-MWNT nanocomposites. Macromol Rapid Commun 2007;28:834–41.
[19] Saito R, Takeya T, Kimura T, Dresselhaus G, Dresselhaus MS. Raman intensity of single-wall carbon nanotubes. Phys Rev B 1998;57:4145–53.
[20] Kurti J, Kresse G, Kuzmany H. First-principles calculations of the radial breathing mode of single-wall carbon nanotubes. Phys Rev B 1998;58:R8869–72.
[21] Kasuya A, Sugano M, Maeda T, Saito Y, Tohji K, Takakashi H, et al. Resonant Raman scattering and the zone-folded electronic structure in single-wall nanotubes. Phys Rev B 1998;57:4999–5001.
[22] Pimenta MA, Marucci A, Empedocles SA, Bawendi MG, Hanlon EB, Rao AM, et al. Raman modes of metallic carbon nanotubes. Phys Rev B 1998;58:R16016–9.

[23] Dresselhaus MS, Dresselhaus G, Saito R, Jorio A. Raman spectroscopy of carbon nanotubes. Phys Rep 2005;49:47–99.
[24] Valentini L, Biagiotti J, Kenny JM, Santucci S. Effects of single-walled carbon nanaotubes on the crystallization behavior of polypropylene. J Appl Polym Sci 2003;87:708–13.
[25] Puglia D, Valentini L, Kenny JM. Analysis of the cure reaction of carbon nanotubes/epoxy resin composites through thermal analysis and Raman spectroscopy. J Appl Polym Sci 2003;88:452–8.
[26] McNally T, Potschke P, Halley P, Murphy M, Martin D, Bell SEJ, et al. Polyethylene multiwalled carbon nanotube composites. Polymer 2005;46:8222–32.
[27] Gojny FH, Wichmann MHG, Fielder B, Kinloch IA, Bauhofer W, Windle AH, et al. Evaluation and identification of electrical and thermal conduction mechanisms in carbon nanotube/epoxy composites. Polymer 2006;47:2036–45.
[28] Assouline E, Lustiger A, Barber AH, Cooper CA, Klein E, Wachtel E, et al. Nucleation ability of multiwall carbon nanotubes in polypropylene composites. J Polym Sci Part B: Polym Phys 2003;41:520–7.
[29] Ganß M, Satapathy BK, Thunga M, Weidisch R, Pötschke P, Janke A. Temperature dependence of creep behavior of PP–MWNT nanocomposites. Macromol Rapid Commun 2007;28:1624–33.
[30] Pötschke P, Krause B, Stange J, Münstedt H. Elongational viscosity and foaming behavior of PP modified by electron irradiation or nanotube addition. Macromol Symp 2007;254:400–8.
[31] Liu T, Phang IY, Shen L, Chow SY, Zhang WD. Morphology and mechanical properties of multiwalled carbon nanotubes reinforced nylon-6 composites. Macromolecules 2004;37:7214–22.
[32] Phang IY, Ma J, Shen L, Liu T, Zhang WD. Crystallization and melting behavior of multi-walled carbon nanotube-reinforced nylon-6 composites. Polym Int 2006;55:71–9.
[33] Li J, Fang Z, Tong L, Gu A, Liu F. Polymorphism of nylon-6 in multiwalled carbon nanotubes/nylon-6 composites. J Polym Sci Part B: Polym Phys 2006;44:1499–512.
[34] Logakis E, Pandis Ch, Peoglos V, Pissis P, Stergiou Ch, Pionteck J, et al. Structure–property relationships in polyamide6/multi-walled carbon nanotubes nanocomposites. J Polym Sci Part B: Polym Phys 2009;47:764–74.
[35] Hiong X, Gao Y, Li HM. Non-isothermal crystallization kinetics of syndiotactic polystyrene–polystyrene functionalized SWNTs nanocomposites. Exp Polym Lett 2007;1:416–26.
[36] Brandrup J, Immergut EH, Grulke EA, Abe A, Bloch DR. Polymer handbook. John Wiley & Sons; 1999.
[37] Gedde W. Polymer physics. London: Chapman & Hall; 1995. p. 154.
[38] Cai Y, Petermann J, Wittich HJ. The oriented growth of iPP spherulites and iPP transcrystallites in thermal gradients. Mater Sci Lett 1995;14:1773–6.
[39] Feldman A, Gonzalez MF, Marom G. Transcrystallinity in surface modified aramid fiber reinforced nylon 66 composites. Macromol Mater Eng 2003;288:861–6.
[40] Peoglos V, Logakis E, Pandis Ch, Pissis P, Pionteck J, Pötschke P, et al. Thermal and electrical characterization of multi-walled carbon nanotubes reinforced polyamide 6 nanocomposites. J Nanostruct Polym Nanocompos 2007;3:116–24.
[41] Zhang S, Minus ML, Zhu L, Wong CP, Kumar S. Polymer transcrystallinity induced by carbon nanotubes. Polymer 2008;49:1356–64.
[42] Lu K, Grossiord N, Koning CE, Miltner HE, Mele B, Loos J. Carbon nanotube/isotactic polypropylene composites prepared by latex technology: morphology analysis of CNT-induced nucleation. Macromolecules 2008;41:8081–5.
[43] Coleman JN, Cadek M, Ryan KP, Fonseca A, Nagy JB, Blau WJ, et al. Reinforcement of polymers with carbon nanotubes. The role of an ordered polymer interfacial region. Experiment and modelling. Polymer 2006;47:8556–61.
[44] Stauffer D. Introduction to percolation theory. 2nd rev. ed. London: Taylor and Francis; 1985. p.91.
[45] Gingold BD, Lobb CJ. Percolative conduction in three dimensions. Phys Rev B 1990;42:8220–4.
[46] Logakis E, Pandis Ch, Peoglos V, Pissis P, Pionteck J, Pötschke P, et al. Electrical/dielectric properties and conduction mechanism in melt processed polyamide/multi-walled carbon nanotubes nanocomposites. Polymer 2009;50:5103–11.
[47] Bergman DJ, Imry Y. Critical behavior of the complex dielectric constant near the percolation threshold of a heterogeneous material. Phys Rev Lett 1977;39:1222–5.
[48] Wang L, Dang ZM. Carbon nanotube composites with high dielectric constant at low percolation threshold. Appl Phys Lett 2005;87:42903.
[49] Li YJ, Xu M, Feng JQ, Dang ZM. Dielectric behavior of a metal–polymer composite with low percolation threshold. Appl Phys Lett 2006;89:72902.
[50] King JA, Johnson BA, Via MD, Ciarkowski CJ. Electrical conductivity of carbon-filled polypropylene-based resins. J Appl Polym Sci 2009;112:425–33.
[51] Lin B, Sundararaj U, Pötschke P. Melt mixing of polycarbonate with multi-walled carbon nanotubes in miniature mixers. Macromol Mater Eng 2006;291:227–38.